Available online at www.sciencedirect.com
SCIENCE DIRECT®
Journal of Sound and Vibration 268 (2003) 149–165
JOURNAL OF SOUND AND VIBRATION
www.elsevier.com/locate/jsvi

# Dynamic stability of spinning pretwisted beams subjected to axial random forces

T.H. Young*, C.Y. Gau

*Department of Mechanical Engineering, National Taiwan University of Science and Technology, 43 Keelung Road, Section 4, Taipei 106, Taiwan*

Received 26 October 2001; accepted 11 November 2002

**Abstract**

This paper studies the dynamic stability of a pretwisted cantilever beam spinning along its longitudinal axis and subjected to an axial random force at the free end. The axial force is assumed as the sum of a constant force and a random process with a zero mean. Due to this axial force, the beam may experience parametric random instability. In this work, the finite element method is first applied to yield discretized system equations. The stochastic averaging method is then adopted to obtain Ito's equations for the response amplitudes of the system. Finally the mean-square stability criterion is utilized to determine the stability condition of the system. Numerical results show that the stability boundary of the system converges as the first three modes are taken into calculation. Before the convergence is reached, the stability condition predicted is not conservative enough.


## 1. Introduction

A vast majority of various products in the world have a variety of holes. Therefore, holemaking is one of the most frequently encountered operations in manufacturing. The common method of generating a hole in materials is by drilling. In a drilling process, the cutting parameters, such as the drill geometry, rotational speed, feed, thrust force, etc., will affect wear and breakage of the drill and accuracy of the hole. Consequently, dynamic behavior of drills has been an important research topic.

The twist drill has a fluted helix angle and two orthogonal principal axes with different cross-sectional area of moments and can be regarded as a pretwisted beam. There exist already a lot of

*Corresponding author. Tel.: +886-2-2737-6444; fax: +886-2-2737-6460.
*E-mail address:* thyoung@mail.ntust.edu.tw (T.H. Young).

0022-460X/03/$ - see front matter 
doi:10.1016/S0022-460X(02)01490-6

references pertaining to the vibration of pretwisted beams. Most of the works [1–5] concerned the vibration of turbine blades and propellers, which are treated as pretwisted, tapered cantilever beams rotating about the axis perpendicular to the longitudinal axis of the beam, and dealt primarily with the determination of natural frequencies and mode shapes of pretwisted beams.

When dealing with dynamic behavior of helical fluted cutters, axial forces have to be included. Magrab and Gilsinn [6] calculated the natural frequencies of a clamped–clamped pretwisted beam under a static axial force by the Galerkin method. Tekinalp and Ulsoy [7,8] investigated the free vibration of drill bits. In these two papers, the fluted cutters are considered as pretwisted beams, and the cutting parameters, such as the pretwist angle, cross-sectional geometry, axial force, rotating speed and feed rate of cutters, are included in the finite element equations. An extensive study of the elastic stability of spinning pretwisted beams subjected to conservative axial forces was presented by Liao and Dang [9].

The axial force considered in the above references is constant. However, the axial force fluctuates within a small range of variation under external disturbances during service. Therefore, it would be more general and realistic to consider a time-dependent axial force for helical fluted cutters. Liao and Huang [10] analyzed the parametric stability of spinning pretwisted beams under periodic axial forces. Summed-type resonances are shown to exist due to this time-varying axial force. Actually, the time-dependent axial force is often of random nature. Consequently, this work extends Liao and Huang's efforts further to study the dynamic stability of spinning pretwisted beams subjected to axial random forces.

## 2. Equations of motion

Fig. 1. shows a schematic view of a pretwisted, cantilever beam of length $L$ spinning along its longitudinal axis with a spin rate $\Omega_0$ and subjected to an axial force $P$ at its free end. In this figure, $(X, Y, Z)$ is a fixed co-ordinate system, while $(x, y, z)$ is a rotating co-ordinate system attached to the beam with the $x$-axis aligned with the $X$-axis. The $(x', y', z')$ co-ordinate system rotates along the longitudinal axis of the beam with a total pretwist angle $\gamma$ such that the $y'$- and $z'$-axes coincide with the principal axes of the pretwisted beam at every cross-section.

If every cross-section of the beam is symmetric with respect to two principal axes of inertia, torsional coupling will not be presented, and only flexural bending is about to occur. In addition, flexural bending takes place simultaneously in two mutually perpendicular planes with unequal flexural rigidities in these two principal axes, and coupling arises due to the presence of the pretwist angle [3]. Thus, the displacement field in the beam can be written as

$$\begin{aligned} u_x(x, y, z, t) &= -y\frac{\partial v}{\partial x} - z\frac{\partial w}{\partial x}, \\ u_y(x, y, z, t) &= v(x, t), \\ u_z(x, y, z, t) &= w(x, t), \end{aligned} \tag{1}$$

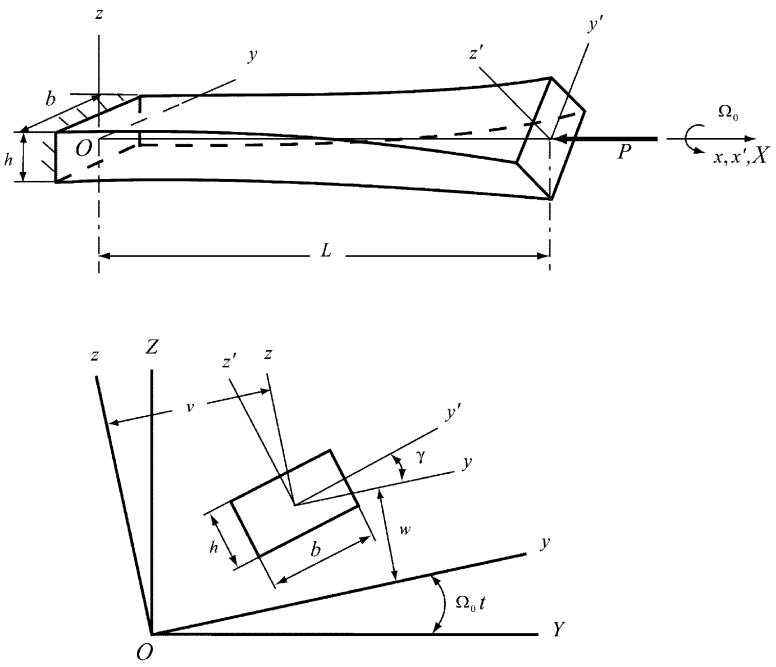


Fig. 1. A schematic view of a spinning pretwisted, cantilever beam subjected to an axial force at its free end.

where $v$ and $w$ are the displacement components of the neutral axis of the beam along the $y$- and $z$-axes, respectively. The strain energy is found to be

$$U = \frac{1}{2}\int_0^L E\left[I_{zz}\left(\frac{\partial^2 v}{\partial x^2}\right)^2 + 2I_{yz}\left(\frac{\partial^2 v}{\partial x^2}\right)\left(\frac{\partial^2 w}{\partial x^2}\right) + I_{yy}\left(\frac{\partial^2 w}{\partial x^2}\right)^2\right] \mathrm{d}x, \tag{2}$$

where $E$ is Young's modulus of the beam; $I_{yy}$, $I_{zz}$ and $I_{yz}$ are the moments and product of area of the beam, respectively. $I_{yy}$, $I_{zz}$ and $I_{yz}$ are related to the moments of area about two principal axes $I_{y'y'}$, and $I_{z'z'}$ at every cross-section by

$$\begin{aligned} I_{yy} &= I_{y'y'}\cos^2(\gamma x/L) + I_{z'z'}\sin^2(\gamma x/L),\\ I_{zz} &= I_{z'z'}\cos^2(\gamma x/L) + I_{y'y'}\sin^2(\gamma x/L),\\ I_{yz} &= \tfrac{1}{2}(I_{z'z'} - I_{y'y'})\sin 2(\gamma x/L). \end{aligned} \tag{3}$$

The work done by the axial force applied at the free end of the beam is given by

$$W_k = -\frac{1}{2}\int_0^L P\left[\left(\frac{\partial v}{\partial x}\right)^2 + \left(\frac{\partial w}{\partial x}\right)^2\right] \mathrm{d}x. \tag{4}$$

The velocity components of a typical point in the beam can be expressed as

$$V_x = -y\frac{\partial^2 v}{\partial t\partial x} - z\frac{\partial^2 w}{\partial t\partial x},$$
$$V_y = \frac{\partial v}{\partial t} - \Omega_0(w+z),$$
$$V_z = \frac{\partial w}{\partial t} + \Omega_0(v+y). \tag{5}$$

Therefore, the kinetic energy due to bending vibration becomes

$$T = \frac{1}{2}\int_0^L \rho\left\{I_{zz}\left[\left(\frac{\partial^2 v}{\partial t\partial x}\right)^2 + \Omega_0^2\right] + 2I_{yz}\left(\frac{\partial^2 v}{\partial t\partial x}\right)\left(\frac{\partial^2 w}{\partial t\partial x}\right) + I_{yy}\left[\left(\frac{\partial^2 w}{\partial t\partial x}\right)^2 + \Omega_0^2\right] + A\left[\left(\frac{\partial v}{\partial t} - \Omega_0 w\right)^2 + \left(\frac{\partial w}{\partial t} + \Omega_0 v\right)^2\right]\right\} \mathrm{d}x, \tag{6}$$

where $\rho$ and $A$ are the mass density and the cross-sectional area of the beam, respectively. If the damping in the beam is of viscous type, by extended Hamilton's principle, the Lagrange equations of motion and the associated boundary conditions can be derived as follows:

Equations of motion:

$$\rho\left[A\left(\frac{\partial^2 v}{\partial t^2} - 2\Omega_0\frac{\partial w}{\partial t} - \Omega_0^2 v\right) - \frac{\partial}{\partial x}\left(I_{zz}\frac{\partial^3 v}{\partial t^2\partial x} + I_{yz}\frac{\partial^3 w}{\partial t^2\partial x}\right)\right] + c\frac{\partial v}{\partial t} + E\frac{\partial^2}{\partial x^2}\left(I_{zz}\frac{\partial^2 v}{\partial x^2} + I_{yz}\frac{\partial^2 w}{\partial x^2}\right) + P(t)\frac{\partial^2 v}{\partial x^2} = 0,$$
$$\rho\left[A\left(\frac{\partial^2 w}{\partial t^2} + 2\Omega_0\frac{\partial v}{\partial t} - \Omega_0^2 w\right) - \frac{\partial}{\partial x}\left(I_{yz}\frac{\partial^3 v}{\partial t^2\partial x} + I_{yy}\frac{\partial^3 w}{\partial t^2\partial x}\right)\right] + c\frac{\partial w}{\partial t} + E\frac{\partial^2}{\partial x^2}\left(I_{yz}\frac{\partial^2 v}{\partial x^2} + I_{yy}\frac{\partial^2 w}{\partial x^2}\right) + P(t)\frac{\partial^2 w}{\partial x^2} = 0, \tag{7}$$

where $c$ is the viscous damping coefficient of the beam.

Boundary conditions:

$$\text{at } x = 0: \quad v = w = \frac{\partial v}{\partial x} = \frac{\partial w}{\partial x} = 0,$$
$$\text{at } x = L: \quad E\left(I_{zz}\frac{\partial^2 v}{\partial x^2} + I_{yz}\frac{\partial^2 w}{\partial x^2}\right) = 0, \quad E\left(I_{yz}\frac{\partial^2 v}{\partial x^2} + I_{yy}\frac{\partial^2 w}{\partial x^2}\right) = 0,$$
$$E\frac{\partial}{\partial x}\left(I_{zz}\frac{\partial^2 v}{\partial x^2} + I_{yz}\frac{\partial^2 w}{\partial x^2}\right) + P\frac{\partial v}{\partial x} - \rho\left(I_{zz}\frac{\partial^3 v}{\partial t^2\partial x} + I_{yz}\frac{\partial^3 w}{\partial t^2\partial x}\right) = 0,$$
$$E\frac{\partial}{\partial x}\left(I_{yz}\frac{\partial^2 v}{\partial x^2} + I_{yy}\frac{\partial^2 w}{\partial x^2}\right) + P\frac{\partial w}{\partial x} - \rho\left(I_{yz}\frac{\partial^3 v}{\partial t^2\partial x} + I_{yy}\frac{\partial^3 w}{\partial t^2\partial x}\right) = 0. \tag{8}$$

Eq. (7) is a set of partial differential equations with time-dependent coefficients and cannot be solved directly.

## 3. Finite element formulation

Initially, dependence on the spatial co-ordinates must be eliminated first from Eq. (7), yielding a set of ordinary differential equations in time which can be solved for system response. Due to the complexity in geometry, the eigensolutions of a pretwisted beam cannot be found exactly [2]. Consequently, an approximate method has to be used to separate the spatial co-ordinate from the temporal variable. In this work, the finite element method is adopted to do this job. Since the two equations of motion are coupled and include the fourth order derivatives with respect to the spatial co-ordinate $x$, the nodal variables should contain two nodal displacements ($v$, $w$) and two nodal slopes ($\partial v/\partial x$, $\partial w/\partial x$). For a two-noded element, the displacement field within the element is interpolated by

$$v(x,\ t) = \sum_{j=1}^{4} d_j(t)\psi_j(x),$$
$$w(x,\ t) = \sum_{j=1}^{4} e_j(t)\psi_j(x), \tag{9}$$

where $d_j$ and $e_j$ are nodal parameters containing ($v$, $\partial v/\partial x$) and ($w$, $\partial w/\partial x$) at each node, respectively; $\psi_j(x)$ are the Hermite cubic interpolation functions.

Substituting the displacement field into the equations of motion and going through the Galerkin procedure yields the finite element model of Eq. (7) for each element:

$$\mu^2[M^e]\begin{Bmatrix}\ddot{\mathbf{d}}\\ \ddot{\mathbf{e}}\end{Bmatrix} + 2\mu^2\Omega_0([G^e]+\alpha[C^e])\begin{Bmatrix}\dot{\mathbf{d}}\\ \dot{\mathbf{e}}\end{Bmatrix} + ([K^e]+P^*[Q^e])\begin{Bmatrix}\mathbf{d}\\ \mathbf{e}\end{Bmatrix} = \mathbf{0}, \tag{10}$$

where $\mu = \sqrt{\rho AL^4/EI_0}$, $\alpha = c/2\rho A\Omega_0$, $P^* = PL^2/EI_0$, in which $I_0$ is the moment of area about the $z$-axis at the clamped end. $\{{}^{\mathbf{d}}_{\mathbf{e}}\}$ is a column matrix formed by all $d_j$ and $e_j$, and a overdot denotes a differentiation with respect to time $t$. The element matrices $[M^e]$, $[G^e]$, $[C^e]$, $[K^e]$ and $[Q^e]$ have the following forms:

$$[M^e] = \begin{bmatrix}[M_1]+[M_2] & [M_4]\\ [M_4] & [M_1]+[M_3]\end{bmatrix},\quad [G^e] = \begin{bmatrix}[0] & -[M_1]\\ [M_1] & [0]\end{bmatrix},$$
$$[C^e] = \begin{bmatrix}[M_1] & [0]\\ [0] & [M_1]\end{bmatrix},\quad [K^e] = \begin{bmatrix}[K_1]-\mu^2\Omega_0^2[M_1] & [K_3]\\ [K_3] & [K_2]-\mu^2\Omega_0^2[M_1]\end{bmatrix},$$
$$[Q^e] = \begin{bmatrix}[K_4] & [0]\\ [0] & [K_4]\end{bmatrix},$$

in which the matrices $[M_1]$, $[M_2]$, $[M_3]$, $[M_4]$, $[K_1]$, $[K_2]$, $[K_3]$ and $[K_4]$ are all symmetric and are defined as follows:

$$M_{ij}^1 = \int_{x_e}^{x_{e+1}} \frac{1}{L}\psi_i\psi_j \,\mathrm{d}x, \quad M_{ij}^2 = \int_{x_e}^{x_{e+1}} \frac{I_{zz}}{AL}\frac{\partial\psi_i}{\partial x}\frac{\partial\psi_j}{\partial x}\,\mathrm{d}x,$$

$$M_{ij}^3 = \int_{x_e}^{x_{e+1}} \frac{I_{yy}}{AL}\frac{\partial\psi_i}{\partial x}\frac{\partial\psi_j}{\partial x}\,\mathrm{d}x, \quad M_{ij}^4 = \int_{x_e}^{x_{e+1}} \frac{I_{yz}}{AL}\frac{\partial\psi_i}{\partial x}\frac{\partial\psi_j}{\partial x}\,\mathrm{d}x,$$

$$K_{ij}^1 = \int_{x_e}^{x_{e+1}} \frac{I_{zz}}{I_0}L^3\frac{\partial^2\psi_i}{\partial x^2}\frac{\partial^2\psi_j}{\partial x^2}\,\mathrm{d}x, \quad K_{ij}^2 = \int_{x_e}^{x_{e+1}} \frac{I_{yy}}{I_0}L^3\frac{\partial^2\psi_i}{\partial x^2}\frac{\partial^2\psi_j}{\partial x^2}\,\mathrm{d}x,$$

$$K_{ij}^3 = \int_{x_e}^{x_{e+1}} \frac{I_{yz}}{I_0}L^3\frac{\partial^2\psi_i}{\partial x^2}\frac{\partial^2\psi_j}{\partial x^2}\,\mathrm{d}x \quad K_{ij}^4 = -\int_{x_e}^{x_{e+1}} L\frac{\partial\psi_i}{\partial x}\frac{\partial\psi_j}{\partial x}\,\mathrm{d}x,$$

where $M_{ij}^1$, $M_{ij}^2$, $M_{ij}^3$, $M_{ij}^4$, $K_{ij}^1$, $K_{ij}^2$, $K_{ij}^3$ and $K_{ij}^4$ are the *i–jth* entries of $[M_1]$, $[M_2]$, $[M_3]$, $[M_4]$, $[K_1]$, $[K_2]$, $[K_3]$ and $[K_4]$, respectively, and the integrations are performed over an element. Note that the matrices $[M^e]$, $[C^e]$, $[K^e]$ and $[Q^e]$ are symmetric, while $[G^e]$ is skew-symmetric. After assembling the element equations and non-dimensionalizing the equation by introducing a non-dimensional temporal variable $\tau = t/\mu$, the discretized equation for the spinning pretwisted beam can be written as

$$[M]\mathbf{\Delta}'' + 2\mu\Omega_0([G] + \alpha[C])\mathbf{\Delta}' + ([\mathrm{K}] + \mathrm{P}^*[\mathrm{Q}])\mathbf{\Delta} = 0, \tag{11}$$

where $[M]$, $[G]$, $[C]$, $[K]$ and $[Q]$ are the mass, gyroscopic, damping, elastic stiffness and geometric stiffness matrices, respectively. $\mathbf{\Delta}$ is a column matrix formed by all the nodal parameters, and a prime denotes a differentiation with respect to $\tau$.

Eq. (11) is a set of second order ordinary differential equations with variable coefficients. To improve the solvability of Eq. (11), a modal analysis suitable for gyroscopic systems is applied to uncouple the undamped, autonomous terms in the system equation. If the axial force can be expressed as the sum of a constant force $P_0$ and a weakly stationary random process with a zero mean $P_1(\tau)$, i.e., $P^*(\tau) = P_0 + P_1(\tau)$. Eq. (11) can be rewritten into a set of first order differential equations of the form

$$\begin{bmatrix} [M] & [0] \\ [0] & [K_t] \end{bmatrix}\mathbf{p}' + \begin{bmatrix} 2\mu\Omega_0[G] & [K_t] \\ -[K_t] & [0] \end{bmatrix}\mathbf{p} = -\left(2\alpha\begin{bmatrix} \mu\Omega_0[C] & [0] \\ [0] & [0] \end{bmatrix} + \mathrm{P}_1(\tau)\begin{bmatrix} [0] & [Q] \\ [0] & [0] \end{bmatrix}\right)\mathbf{p}, \tag{12}$$

where $[K_t] = [K] + P_0[Q]$ and $\mathbf{p} = \{^{\mathbf{\Delta}'}_{\mathbf{\Delta}}\}$ The eigenvalues of the corresponding undamped, autonomous system of Eq. (12) appear in complex conjugate pairs, i.e., $\lambda_n = \pm \mathrm{i}\omega_n$, $n = 1, 2, \ldots, N$, where $\omega_n$ are the non-dimensionalized natural frequencies of the pretwisted beam, and $N$ is the total degrees of freedom of the discretized system. The eigenvectors of the corresponding undamped, autonomous system of Eq. (12) also appear in complex conjugate pairs, i.e., $\mathbf{x}_n = \mathbf{y}_n + \mathrm{i}\mathbf{z}_n$, $\bar{\mathbf{x}}_n = \mathbf{y}_n - \mathrm{i}\mathbf{z}_n$, where $\mathbf{y}_n$ and $\mathbf{z}_n$ are the real and imaginary parts of the eigenvector $\mathbf{x}_n$, respectively.

In order to save computation efforts, a modal truncation method is utilized. Introduce a linear transformation $\mathbf{p} = [P]\zeta$, where $[P]$ is the matrix formed by the real and imaginary parts of the first

$J$ normalized eigenvectors of the system. Substituting this transformation into Eq. (12), premultiplying the transpose of $[P]$ and using the orthogonality of eigenvectors yields the following partially uncoupled equation:

$$\zeta' + [\Lambda]\zeta = -2\alpha[C^*]\zeta - \frac{P_1(\tau)}{P_0}[Q^*]\zeta, \tag{13}$$

where $[\Lambda]$ is a block diagonal matrix of the form

$$[\Lambda] = \text{block-diag.}\begin{bmatrix} 0 & -\omega_n \\ \omega_n & 0 \end{bmatrix}, \quad [C^*] = [P]^{\mathrm{T}}\begin{bmatrix} \mu\Omega_0[C] & [0] \\ [0] & [0] \end{bmatrix}[P], \quad [Q^*] = P_0[P]^{\mathrm{T}}\begin{bmatrix} [0] & [Q] \\ [0] & [0] \end{bmatrix}[P].$$

Again $[C^*]$ is symmetric due to the property of the congruent transformation. The terms on the left-hand side of Eq. (13) are uncoupled in a blockwise sense; however, those on the right-hand side of the equation are still coupled together. To match the form of the matrix $[\Lambda]$, the matrices on the right-hand side are partitioned into $J^2$ blocks of $2 \times 2$ matrices. Hence, Eq. (13) can be rewritten into the following form:

$$\begin{aligned} \xi_n' - \omega_n\eta_n &= -2\alpha\sum_{j=1}^{J}(c_{nj}^{11}\xi_j + c_{nj}^{12}\eta_j) - \frac{P_1(\tau)}{P_0}\sum_{j=1}^{J}(q_{nj}^{11}\xi_j + q_{nj}^{12}\eta_j), \\ \eta_n' + \omega_n\xi_n &= -2\alpha\sum_{j=1}^{J}(c_{nj}^{21}\xi_j + c_{nj}^{22}\eta_j) - \frac{P_1(\tau)}{P_0}\sum_{j=1}^{J}(q_{nj}^{21}\xi_j + q_{nj}^{22}\eta_j), \\ n &= 1, 2, \ldots, J, \end{aligned} \tag{14}$$

where $\xi_n$ and $\eta_n$ are the $(2n-1)$th and $2n$th entries of $\zeta$; $c_{nj}^{ik}$ and $q_{nj}^{ik}$ are the $i$–$k$th entries of the $n$–$j$th blocks of $[C^*]$ and $[Q^*]$, respectively.

## 4. Stochastic averaging method

The solutions of Eq. (14) are assumed to be of the form

$$\xi_n = a_n\cos\Phi_n, \quad \eta_n = -a_n\sin\Phi_n, \quad n = 1, 2, \ldots, J, \tag{15}$$

where $\Phi_n = \omega_n\tau + \phi_n$, in which $a_n$ and $\phi_n$ are amplitudes and phase angles of the system response, respectively. Substituting Eq. (15) into Eq. (14) yields

$$\begin{aligned} a_n' &= f_{an}(\mathbf{a}, \boldsymbol{\phi}) + \frac{P_1(\tau)}{P_0}g_{an}(\mathbf{a}, \boldsymbol{\phi}), \\ \phi_n' &= f_{\phi n}(\mathbf{a}, \boldsymbol{\phi}) + \frac{P_1(\tau)}{P_0}g_{\phi n}(\mathbf{a}, \boldsymbol{\phi}), \quad n = 1, 2, \ldots, J, \end{aligned} \tag{16}$$

where

$$f_{an}(\mathbf{a},\,\boldsymbol{\phi}) = \alpha\sum_{j=1}^{J}(-c_{nj}^{11}\cos\Phi_n\cos\Phi_j + c_{nj}^{12}\cos\Phi_n\sin\Phi_j + c_{nj}^{21}\sin\Phi_n\cos\Phi_j - c_{nj}^{22}\sin\Phi_n\sin\Phi_j)a_j,$$

$$g_{an}(\mathbf{a},\,\boldsymbol{\phi}) = \sum_{j=1}^{J}(-q_{nj}^{11}\cos\Phi_n\cos\Phi_j + q_{nj}^{12}\cos\Phi_n\sin\Phi_j + q_{nj}^{21}\sin\Phi_n\cos\Phi_j - q_{nj}^{22}\sin\Phi_n\sin\Phi_j)a_j,$$

$$f_{\phi n}(\mathbf{a},\,\boldsymbol{\phi}) = \alpha\sum_{j=1}^{J}(c_{nj}^{11}\sin\Phi_n\cos\Phi_j - c_{nj}^{12}\sin\Phi_n\sin\Phi_j + c_{nj}^{21}\cos\Phi_n\cos\Phi_j - c_{nj}^{22}\cos\Phi_n\sin\Phi_j)\frac{a_j}{a_n},$$

$$g_{\phi n}(\mathbf{a},\,\boldsymbol{\phi}) = \sum_{j=1}^{J}(q_{nj}^{11}\sin\Phi_n\cos\Phi_j - q_{nj}^{12}\sin\Phi_n\sin\Phi_j + q_{nj}^{21}\cos\Phi_n\cos\Phi_j - q_{nj}^{22}\cos\Phi_n\sin\Phi_j)\frac{a_j}{a_n},$$

where $\mathbf{a}$ and $\boldsymbol{\phi}$ are column matrices formed by all $a_n$ and $\phi_n$, respectively.

Assume that the damping ratio $\alpha$ and the random excitation $P_1(\tau)$ are small in some sense such that $\alpha$ is of order $\varepsilon$, and $P_1(\tau)/P_0$ is of order $\varepsilon^{1/2}$, where $\varepsilon$ is a small parameter. Hence, the stochastic averaging procedure can be applied to Eq. (16), and $\{{\mathbf{a}\atop\boldsymbol{\phi}}\}$ can be uniformly approximated in the weak sense by a Markov vector [11]

$$\begin{aligned} \mathrm{d}a_n &= m_n\,\mathrm{d}t + \sum_{r=1}^{2J}\sigma_{nr}\,\mathrm{d}B_r,\\ \mathrm{d}\phi_n &= m_{(n+J)}\,\mathrm{d}t + \sum_{r=1}^{2J}\sigma_{(n+J)r}\,\mathrm{d}B_r, \quad n = 1,\,2,\,\ldots,\,J, \end{aligned} \tag{17}$$

where $B_r$ are independent unit Wiener processes; $m_j$ are drift coefficients, and $\sigma_{jk}$ are elements of the diffusion matrix $[\sigma]$ with

$$\begin{aligned} m_n &= \left\langle f_{an}(\mathbf{a},\,\boldsymbol{\phi};\,\tau) + \int_{-\infty}^{0}\left\{ g_{aj}(\mathbf{a},\,\boldsymbol{\phi};\,\tau+\tau^*)\frac{\partial}{\partial a_j}g_{an}(\mathbf{a},\,\boldsymbol{\phi};\,\tau),\right.\right.\\ &\quad \left.\left. + g_{\phi j}(\mathbf{a},\,\boldsymbol{\phi};\,\tau+\tau^*)\frac{\partial}{\partial \phi_j}g_{an}(\mathbf{a},\,\boldsymbol{\phi};\,\tau)\right\}R(\tau^*)\,\mathrm{d}\tau^*\right\rangle_\tau,\\ m_{(n+J)} &= \left\langle f_{\phi n}(\mathbf{a},\,\boldsymbol{\phi};\,\tau) + \int_{-\infty}^{0}\left\{ g_{aj}(\mathbf{a},\,\boldsymbol{\phi};\,\tau+\tau^*)\frac{\partial}{\partial a_j}g_{\phi n}(\mathbf{a},\,\boldsymbol{\phi};\,\tau)\right.\right.\\ &\quad \left.\left. +g_{\phi j}(\mathbf{a},\,\boldsymbol{\phi};\,\tau+\tau^*)\frac{\partial}{\partial \phi_j}g_{\phi n}(\mathbf{a},\,\boldsymbol{\phi};\,\tau)\right\}R(\tau^*)\,\mathrm{d}\tau^*\right\rangle_\tau,\\ ([\sigma][\sigma]^{\mathrm{T}})_{jk} &= \left\langle \int_{-\infty}^{\infty} g_{aj}(\mathbf{a},\,\boldsymbol{\phi};\,\tau)g_{ak}(\mathbf{a},\,\boldsymbol{\phi};\,\tau+\tau^*)R(\tau^*)\,\mathrm{d}\tau^*\right\rangle_\tau,\\ ([\sigma][\sigma]^{\mathrm{T}})_{j(k+J)} &\left\langle \int_{-\infty}^{\infty} g_{aj}(\mathbf{a},\,\boldsymbol{\phi};\,\tau)g_{\phi k}(\mathbf{a},\,\boldsymbol{\phi};\,\tau+\tau^*)R(\tau^*)\,\mathrm{d}\tau^*\right\rangle_\tau, \end{aligned}$$

$$([\sigma][\sigma]^{\mathrm{T}})_{(j+J)k}\left\langle \int_{-\infty}^{\infty} g_{\phi j}(\mathbf{a},\,\boldsymbol{\phi};\,\tau)g_{ak}(\mathbf{a},\,\boldsymbol{\phi};\,\tau+\tau^{*})R(\tau^{*})\,d\tau^{*}\right\rangle_{\tau},$$

$$([\sigma][\sigma]^{\mathrm{T}})_{(j+J)(k+J)} = \left\langle \int_{-\infty}^{\infty} g\phi_{j}(\mathbf{a},\,\boldsymbol{\phi};\,\tau)g_{\phi k}(\mathbf{a},\,\boldsymbol{\phi};\,\tau+\tau^{*})R(\tau^{*})\,\mathrm{d}\tau^{*}\right\rangle_{\tau}$$

$$j,\,k=1,\,2,\,\ldots,\,J,$$

where $([\sigma][\sigma]^{\mathrm{T}})_{jk}$ is the $j$–$k$th entry of the product of $[\sigma]$ and its transpose; $R(\tau)$ is the autocorrelation function of $P_1(\tau)/P_0$, and $\langle[\cdot]\rangle_{\tau}$ denotes a time-averaging operation with respect to $\tau$,

$$\langle[\cdot]\rangle_{\tau}=\lim_{T\to\infty}\frac{1}{2T}\int_{-T}^{T}[\cdot]\,\mathrm{d}\tau.$$

Going through the integrations, these coefficients can be obtained. Detailed expressions of these coefficients are given in the Appendix.

The Ito differential equations for $a_n^2$ can be acquired by Ito's differential rule as

$$\mathrm{d}a_n^2=[2m_n a_n+([\sigma][\sigma]^{\mathrm{T}})_{nn}]\,\mathrm{d}\tau+2a_n\sum_{r=1}^{2J}\sigma_{nr}\,\mathrm{d}B_r,\quad n=1,\,2,\,\ldots,\,J. \tag{18}$$

Taking the expectation on both sides of the equation yields

$$\begin{aligned}\frac{\mathrm{d}}{\mathrm{d}\tau}E[a_n^2] = &-2\alpha(c_{nn}^{11}+c_{nn}^{22})E[a_n^2]\\
&+\tfrac{1}{4}\sum_{j=1}^{J}\{(q_{nj}^{11}q_{jn}^{11}+q_{nj}^{22}q_{jn}^{22}+q_{nj}^{12}q_{jn}^{21}+q_{nj}^{21}q_{jn}^{12})[\mathrm{S}(\omega_n-\omega_j)+S(\omega_n+\omega_j)]E[a_n^2]\\
&+(q_{nj}^{11}q_{jn}^{22}+q_{nj}^{22}q_{jn}^{11}-q_{nj}^{12}q_{jn}^{12}-q_{nj}^{21}q_{jn}^{21})[S(\omega_n-\omega_j)-S(\omega_n+\omega_j)]E[a_n^2]\\
&+(q_{nj}^{11}q_{nj}^{11}+q_{nj}^{22}q_{nj}^{22}+q_{nj}^{12}q_{nj}^{12}+q_{nj}^{21}q_{nj}^{21})[S(\omega_n-\omega_j)+S(\omega_n+\omega_j)]E[a_j^2]\\
&+2(q_{nj}^{11}q_{nj}^{22}-q_{nj}^{12}q_{nj}^{21})[S(\omega_n-\omega_j)-S(\omega_n+\omega_j)]E[a_j^2]\\
&+(q_{nj}^{21}q_{jn}^{11}+q_{nj}^{22}q_{jn}^{21}-q_{nj}^{11}q_{jn}^{12}-q_{nj}^{12}q_{jn}^{22})[\Psi(\omega_n-\omega_j)+\Psi(\omega_n+\omega_j)]E[a_n^2]\\
&+(q_{nj}^{12}q_{jn}^{11}+q_{nj}^{22}q_{jn}^{12}-q_{nj}^{11}q_{jn}^{21}-q_{nj}^{21}q_{jn}^{22})[\Psi(\omega_n+\omega_j)-\Psi(\omega_n-\omega_j)]E[a_n^2]\}\\
&+\tfrac{1}{4}(q_{nn}^{12}q_{nn}^{22}+q_{nn}^{21}q_{nn}^{22}-q_{nn}^{11}q_{nn}^{12}-q_{nn}^{11}q_{nn}^{21})\Psi(2\omega_n)]E[a_n^2]\\
&n=1,\,2,\,\ldots,\,J,\end{aligned} \tag{19}$$

where $S(\omega)$ and $\Psi(\omega)$ are defined in the Appendix. Note that in the above equation, $q_{nn}^{11}=-q_{nn}^{22}$ is observed if the matrix [Q] is symmetric. Eq. (19) can be rewritten into a matrix form:

$$\frac{\mathrm{d}}{\mathrm{d}\tau}\delta=[D]\delta, \tag{20}$$

where $\delta=\{E[a_1^2],\,E[a_2^2],\,\ldots,\,E[a_J^2]\}^{\mathrm{T}}$. When all the real parts of eigenvalues of the coefficient matrix $[D]$ are negative, the mean-square response of the system decays with time, and the system is stable in the mean-square sense. When one of the real parts of eigenvalues of the coefficient matrix $[D]$ is positive, the mean-square response of that mode enlarges with time, and the system is unstable in the mean-square sense. Therefore, the mean-square stability boundary of the system

corresponds to the condition such that one of the real parts of eigenvalues of the coefficient matrix $[D]$ becomes zero.

## 5. Numerical results and discussions

Before formally presenting the numerical results for the stability analysis, convergence studies of the finite element model and the modal truncation method have to be conducted first. According to the suggestion by the previous study [9], 25 uniform elements are used to model the spinning pretwisted beam in this work. As an application of the general solution, the random process $P_1(\tau)/P_0$ is assumed as a Gaussian white noise with a spectral density $S$ here for simplicity. Therefore, $S(0) = S(2\omega_n) = S(\omega_j \pm \omega_k) = S$, $\Psi(2\omega_n) = \Psi(\omega_j \pm \omega_k) = 0$. However, the numerical results for other random processes can also be produced easily. In addition, all the numerical results in this work are presented in non-dimensional forms: therefore, $\Omega_0$ in this section represents the non-dimensional expression $\Omega_0/\omega_0$, where $\omega_0$ is the fundamental natural frequency of the free, non-spinning prismatic beam, i.e., $\omega_0 = 3.5156\sqrt{EI_0/\rho AL^4}$.

Fig. 2 presents the effect of the number of modes used in the modal truncation method on the mean-square stability boundary of a spinning pretwisted beam subjected to an axial random force. The mean-square stability boundary on the $S$–$\alpha$ plane is a straight line originated from the origin because all the entries of the coefficient matrix $[D]$ in Eq. (20) are functions of the ratio $S/\alpha$ for a Gaussian white noise $P_1(\tau)/P_0$. The unstable region lies above the stability boundary. As the number of modes $J$ increases from 1, the stability boundary rotates downwards about the origin, leaving a larger unstable region. The stability boundaries for $J$ equal to 3 and 4 almost coincide with each other. A further increase in $J$ cannot make the stability boundary rotate downwards any further. Therefore, with only the first three modes of the beam used in the modal truncation

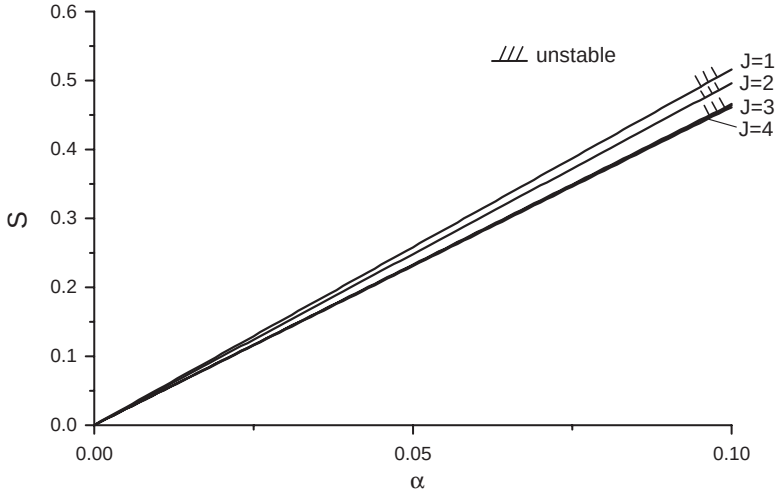


Fig. 2. The effect of the number of modes on the mean-square stability boundary of a spinning pretwisted beam subjected to an axial random force: $L/b = 10$, $R = 0.25$, $\gamma = 90^\circ$, $\Omega_0 = 0.1$, $P_0 = 0.5$.

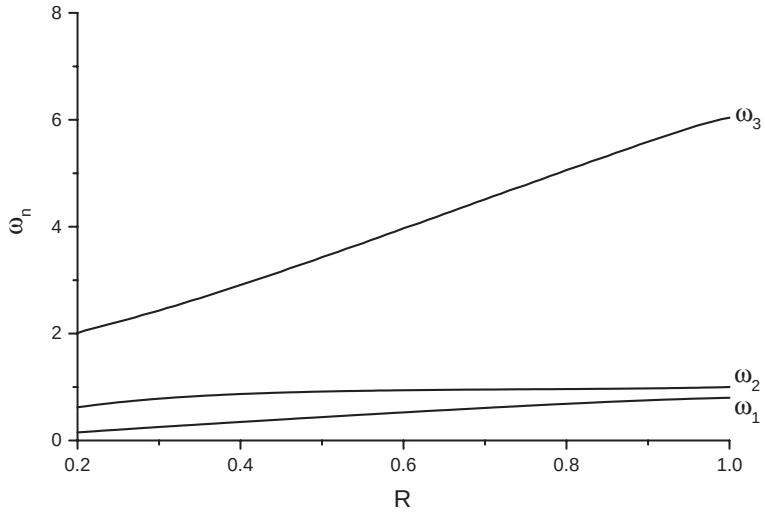


Fig. 3. The first three natural frequencies of a spinning pretwisted beam subjected to a static axial force versus the thickness-to-breadth ration: $L/\sqrt{bh} = 10$, $\gamma = 90^\circ$, $\Omega_0 = 0.1$, $P_0 = 0.5$.

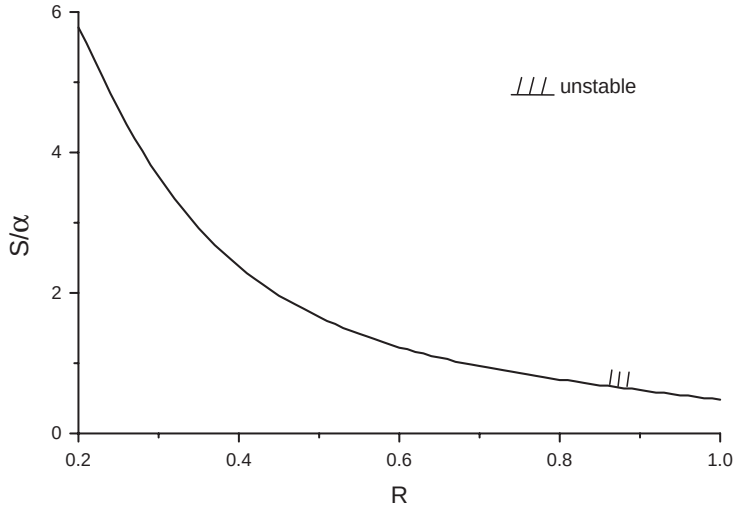


Fig. 4. The effect of the thickness-to-breadth ratio on the mean-square stability boundary of a spinning pretwisted beam subjected to an axial random force: $L/\sqrt{bh} = 10$, $\gamma = 90^\circ$, $\Omega_0 = 0.1$, $P_0 = 0.5$.

method, the mean-square stability boundary of the system converges quickly. Before the convergence is reached, the stability condition predicted is not conservative enough. In addition, the effect of the viscous damping is stabilizing, while the effect of the random part of the axial force is destabilizing.

Parametric studies of the free vibration of the spinning pretwisted beam should be carried out before the systematic investigation of the effects of various parameters on the stability boundary of the beam. Fig. 3 shows the first three natural frequencies of a spinning pretwisted beam

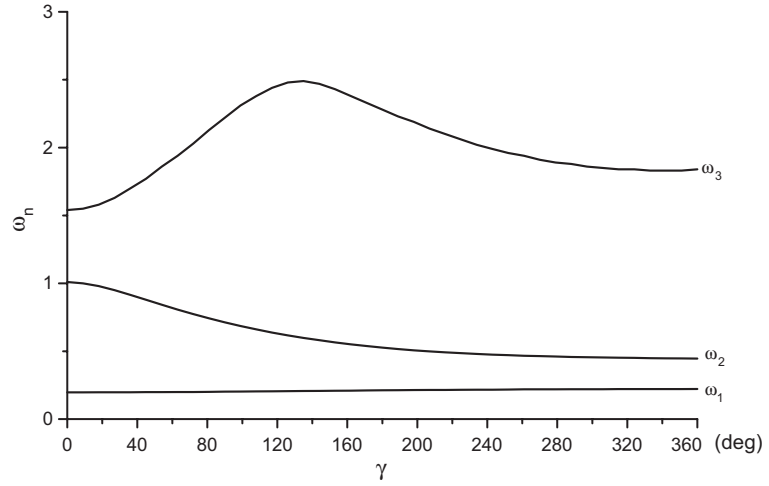


Fig. 5. The first three natural frequencies of a spinning pretwisted beam subjected to a static axial force versus the total pretwist angle: $L/b=10$, $R=0.25$, $\Omega_0=0.1$, $P_0=0.5$.

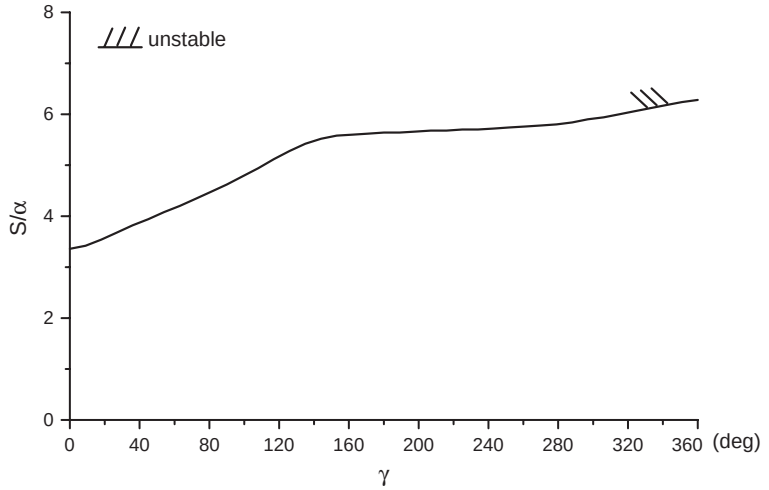


Fig. 6. The effect of the total pretwist angle on the mean-square stability boundary of a spinning pretwisted beam subjected to an axial random force: $L/b=10$, $R=0.25$, $\Omega_0=0.1$, $P_0=0.5$.

subjected to a static axial force under changes of the thickness-to-breadth ratio $R=h/b$. In this figure, the cross-sectional area of the beam $A=bh$ remains constant. It is found that the first three natural frequencies rise as the thickness-to-breadth ratio increases. The effect of the thickness-to-breadth ratio on the mean-square stability boundary of the system is depicted in Fig. 4. Since the mean-square stability boundary depends only on the ratio $S/\alpha$ for a Gaussian white noise $P_1(\tau)/P_0$, the stability boundary is shown on the $(S/\alpha)$–$R$ plane, and the unstable region lies above the stability boundary. As the ratio increases from 0.2 to 1.0, the stability boundary drops down very quickly, leaving a larger unstable region. Consequently, the effect of the thickness-to-breadth

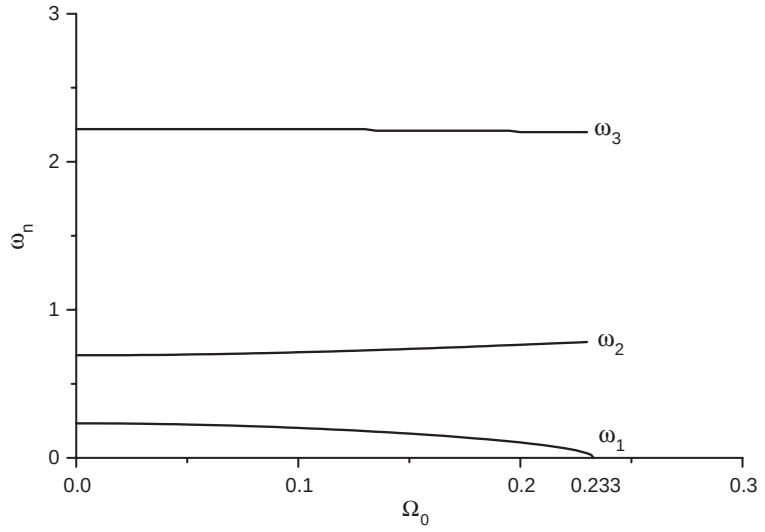


Fig. 7. The first three natural frequencies of a spinning pretwisted beam subjected to a static axial force versus the spin rate: $L/b=10$, $R=0.25$, $\gamma=90^\circ$, $\Omega_0=0.1$, $P_0=0.5$.

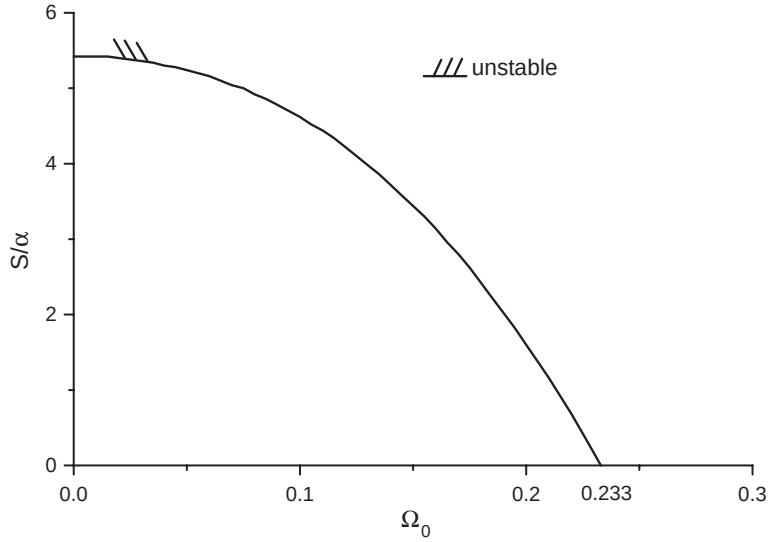


Fig. 8. The effect of the spin rate on the mean-square stability boundary of a spinning pretwisted beam subjected to an axial random force: $L/b=10$, $R=0.25$, $\gamma=90^\circ$, $P_0=0.5$.

ratio within this range is destabilizing in this situation though it will raise the lowest few natural frequencies of the beam.

Fig. 5 illustrates the first three natural frequencies of a spinning pretwisted beam subjected to a static axial force under changes of the total pretwist angle $\gamma$. As $\gamma$ increases from $0^\circ$, the first natural frequency rises a little bit; the second natural frequency lowers significantly, while the third one goes up and down. Fig. 6 shows the mean-square stability boundary of the system

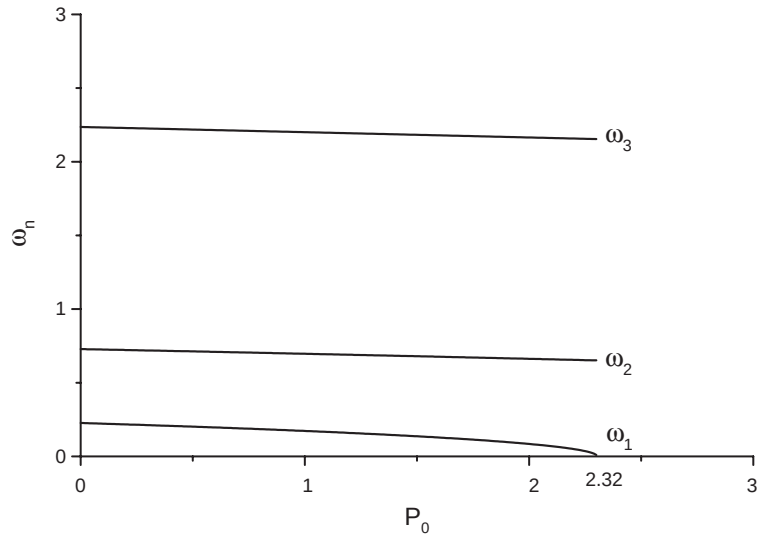


Fig. 9. The first three natural frequencies of a spinning pretwisted beam under changes of the static axial forcer: $L/b=10$, $R=0.25$, $\gamma=90^\circ$, $\Omega_0=0.1$.

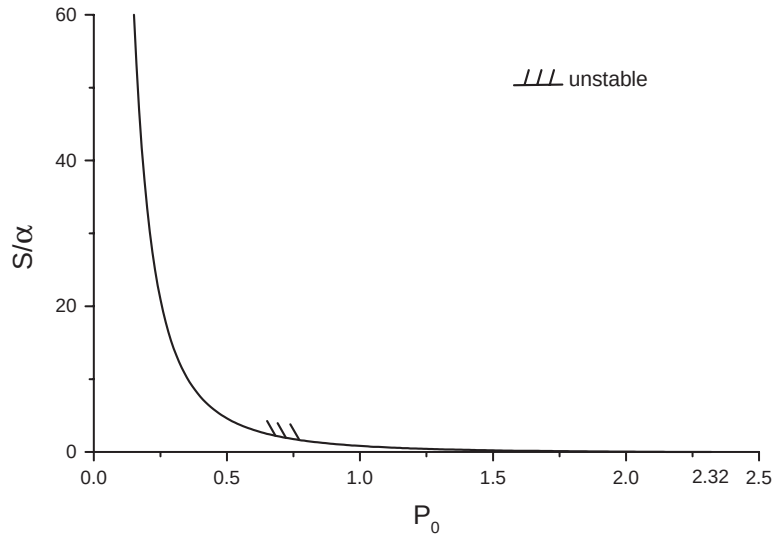


Fig. 10. The effect of the average axial force on the mean-square stability boundary of a spinning pretwisted beam subjected to an axial random force: $L/b=10$, $R=0.25$, $\gamma=90^\circ$, $\Omega_0=0.1$.

on the $(S/\alpha)$–$\gamma$ plane. The boundary rises monotonically at different rates as $\gamma$ increases up to 360°. Hence, the effect of the pretwist angle is stabilizing for a total pretwist angle less than 360°.

The first three natural frequencies of a spinning pretwisted beam subjected to a static axial force versus the spin rate $\Omega_0$ is depicted in Fig. 7. As the spin rate increases, the first natural frequency

decreases; the second natural frequency rises, but the third one is almost unchanged. At $\Omega_0 = 0.233$, where the first natural frequency becomes zero, the beam will experience a divergence-type instability, and this value of $\Omega_0$ is called the critical speed of the beam. Fig. 8 illustrates the effect of the spin rate of the beam on the mean-square stability of the system. The boundary falls down as the spin rate increases. Therefore, the effect of the spin rate is unfavorable to the mean-square stability of the system. Note that the stability boundary touches the abscissa at $\Omega_0 = 0.233$, which is the critical speed of the beam under the action of the static axial load $P_0$, beyond which the system is unstable even if the random part of the axial force is absent.

Fig. 9 presents the first three natural frequencies of a spinning pretwisted beam under changes of the static axial force. All the lowest three natural frequencies reduce as the static axial force increases. At $P_0 = 2.32$ where the first natural frequency becomes zero, the beam will experience a divergence-type instability, and this value of $P_0$ is called the buckling load of the spinning beam. The effect of the average axial force $P_0$ on the mean-square stability of the system is shown in Fig. 10. The boundary drops down drastically as the average axial force increases. Again the effect of the average axial force is undesirable to the mean-square stability of the system. Note that the stability boundary meets the abscissa at $P_0 = 2.32$, which is the buckling load of the spinning pretwisted beam, beyond which the system is unstable even though the random part of the axial force is absent.

## 6. Conclusions

The dynamic stability of a pretwisted cantilever beam spinning along its longitudinal axis and subjected to an axial random force at the free end is analyzed in this work. The axial force is assumed as the sum of a static force and a random process with a zero mean. Due to this axial random force, the beam may experience parametric random instability. In this work, the mean-square stability criterion is utilized to determine the stability condition of the system. Numerical results are given for a Gaussian white noise excitation.

The effects of various system parameters on the mean-square stability boundary of the system were investigated, and the following conclusions can be drawn:

(1) The mean-square stability boundary of the system converges as the first three modes are taken into consideration. Before the convergence is reached, the stability condition predicted is not conservative enough.
(2) The mean-square stability boundary of the system on the $S$-$\alpha$ plane is a straight line originated from the origin because the stability boundary depends only on the ratio $S/\alpha$. The effect of the viscous damping is favorable, but the effect of the random part of the axial force is unfavorable.
(3) For the total pretwist angle $\gamma$ less than $360^\circ$, its effect is stabilizing in the mean-square sense. For the thickness-to-breadth ratio $R$ between 0.2 and 1.0, its effect is destabilizing.
(4) The effects of the spin rate and average axial force tend to destabilize the system, and the mean-square stability boundary will not exist any more once the spin rate (or the average axial force) exceeds the critical speed (or the buckling load).

## Appendix

$$
\begin{aligned}
m_n = & -\alpha(c_{nn}^{11}+c_{nn}^{22})a_n+\tfrac{1}{16}\sum_{r=1}^{J}\Bigg\{\Bigg[2(q_{nr}^{11}q_{rn}^{11}+q_{nr}^{22}q_{rn}^{22}+q_{nr}^{12}q_{rn}^{21}+q_{nr}^{21}q_{rn}^{12})a_n+(q_{nr}^{11}q_{nr}^{11}..\\
&+q_{nr}^{22}q_{nr}^{22}+q_{nr}^{12}q_{nr}^{12}+q_{nr}^{21}q_{nr}^{21})\frac{a_r^2}{a_n}\Bigg][S(\omega_n-\omega_r)+S(\omega_n+\omega_r)]+\Bigg[2(q_{nr}^{11}q_{rn}^{22}+q_{nr}^{22}q_{rn}^{11}.\\
&-q_{nr}^{12}q_{rn}^{12}-q_{nr}^{21}q_{rn}^{21})a_n+2(q_{nr}^{11}q_{nr}^{22}-q_{nr}^{12}q_{nr}^{21})\frac{a_r^2}{a_n}\Bigg][S(\omega_n-\omega_r)-S(\omega_n+\omega_r)]\\
&+\left[2(q_{nr}^{21}q_{rn}^{11}+q_{nr}^{22}q_{rn}^{21}-q_{nr}^{11}q_{rn}^{12}-q_{nr}^{12}q_{rn}^{22})a_n\right][\Psi(\omega_n-\omega_r)+\Psi(\omega_n+\omega_r)]\\
&+[2(q_{nr}^{12}q_{rn}^{11}+q_{nr}^{22}q_{rn}^{12}-q_{nr}^{11}q_{rn}^{21}-q_{nr}^{21}q_{rn}^{22})a_n][\Psi(\omega_n+\omega_r)-\Psi(\omega_n-\omega_r)]\Bigg\}\\
&-\tfrac{1}{16}\{2(q_{nn}^{11}q_{nn}^{22}+q_{nn}^{12}q_{nn}^{21})[S(0)+S(2\omega_n)]\\
&+(q_{nn}^{11}q_{nn}^{11}+q_{nn}^{22}q_{nn}^{22}-q_{nn}^{12}q_{nn}^{12}-q_{nn}^{21}q_{nn}^{21})[S(0)-S(2\omega_n)]\\
&+2(q_{nn}^{12}q_{nn}^{22}+q_{nn}^{21}q_{nn}^{22}-q_{nn}^{11}q_{nn}^{12}-q_{nn}^{11}q_{nn}^{21})\Psi(2\omega_n)\}a_n,
\end{aligned}
$$

$$
\begin{aligned}
m_{(n+J)} = & \tfrac{1}{8}\sum_{r=1}^{J}\{(q_{nr}^{11}q_{rn}^{12}+q_{nr}^{12}q_{rn}^{22}-q_{nr}^{21}q_{rn}^{11}-q_{nr}^{22}q_{rn}^{21})[S(\omega_n-\omega_r)+S(\omega_n+\omega_r)]\\
&+(-q_{nr}^{11}q_{rn}^{21}+q_{nr}^{12}q_{rn}^{11}-q_{nr}^{21}q_{rn}^{22}+q_{nr}^{22}q_{rn}^{12})[S(\omega_n-\omega_r)-S(\omega_n+\omega_r)]\\
&+(q_{nr}^{11}q_{rn}^{11}+q_{nr}^{22}q_{rn}^{22}+q_{nr}^{12}q_{rn}^{21}+q_{nr}^{21}q_{rn}^{12})[\Psi(\omega_n-\omega_r)+\Psi(\omega_n+\omega_r)]\\
&+(-q_{nr}^{11}q_{rn}^{22}+q_{nr}^{12}q_{rn}^{12}-q_{nr}^{22}q_{rn}^{11}+q_{nr}^{21}q_{rn}^{21})[\Psi(\omega_n+\omega_r)-\Psi(\omega_n-\omega_r)]\}\\
&+\tfrac{1}{8}\{2(q_{nn}^{22}q_{nn}^{21}-q_{nn}^{11}q_{nn}^{12})[S(0)+S(2\omega_n)]+2(q_{nn}^{21}q_{nn}^{11}-q_{nn}^{12}q_{nn}^{22})[S(0)-S(2\omega_n)]\\
&+(q_{nn}^{12}q_{nn}^{12}+q_{nn}^{21}q_{nn}^{21}+2q_{nn}^{12}q_{nn}^{21}-q_{nn}^{11}q_{nn}^{11}-q_{nn}^{22}q_{nn}^{22}+2q_{nn}^{11}q_{nn}^{22})\Psi(2\omega_n)\},
\end{aligned}
$$

$$
\begin{aligned}
([\sigma][\sigma]^{\mathrm{T}})_{jk} = & \tfrac{1}{8}\{(q_{jk}^{11}q_{kj}^{11}+q_{jk}^{22}q_{kj}^{22}+q_{jk}^{12}q_{kj}^{21}+q_{jk}^{21}q_{kj}^{12})[S(\omega_j-\omega_k)+S(\omega_j+\omega_k)]\\
&+(q_{jk}^{11}q_{kj}^{22}+q_{jk}^{22}q_{kj}^{11}-q_{jk}^{12}q_{kj}^{12}-q_{jk}^{21}q_{kj}^{21})[S(\omega_j-\omega_k)-S(\omega_j+\omega_k)]\\
&+2(q_{jj}^{11}q_{kk}^{11}+q_{jj}^{11}q_{kk}^{22}+q_{jj}^{22}q_{kk}^{11}+q_{jj}^{22}q_{kk}^{22})S(0)\}a_ja_k,
\end{aligned}
$$

$$
\begin{aligned}
([\sigma][\sigma]^{\mathrm{T}})_{j(k+J)} = & \tfrac{1}{8}\{(-q_{jk}^{11}q_{kj}^{21}+q_{jk}^{22}q_{kj}^{12}+q_{jk}^{12}q_{kj}^{11}-q_{jk}^{21}q_{kj}^{22})[S(\omega_j-\omega_k)+S(\omega_j+\omega_k)]\\
&+(-q_{jk}^{22}q_{kj}^{21}+q_{jk}^{11}q_{kj}^{12}-q_{jk}^{21}q_{kj}^{11}+q_{jk}^{12}q_{kj}^{22})[S(\omega_j-\omega_k)-S(\omega_j+\omega_k)]\\
&+2(-q_{jj}^{11}q_{kk}^{21}+q_{jj}^{22}q_{kk}^{12}-q_{jj}^{22}q_{kk}^{21}+q_{jj}^{11}q_{kk}^{12})S(0)\}a_j,
\end{aligned}
$$

$$
([\sigma][\sigma]^{\mathrm{T}})_{(j+J)k} = ([\sigma][\sigma]^{\mathrm{T}})_{k(j+J)},
$$

$$
\begin{aligned}
([\sigma][\sigma]^{\mathrm{T}})_{(j+J)(k+J)} = & \tfrac{1}{8}\{(q_{jk}^{21}q_{kj}^{21}+q_{jk}^{12}q_{kj}^{12}-q_{jk}^{22}q_{kj}^{11}-q_{jk}^{11}q_{kj}^{22})[S(\omega_j-\omega_k)+S(\omega_j+\omega_k)]\\
&-(q_{jk}^{21}q_{kj}^{12}+q_{jk}^{12}q_{kj}^{21}+q_{jk}^{22}q_{kj}^{22}+q_{jk}^{11}q_{kj}^{11})[S(\omega_j-\omega_k)-S(\omega_j+\omega_k)]\\
&+(q_{jj}^{21}q_{kk}^{21}-q_{jj}^{21}q_{kk}^{12}-q_{jj}^{12}q_{kk}^{21}+q_{jj}^{12}q_{kk}^{12})S(0)\},
\end{aligned}
$$

where $S(\omega)=2\int_0^\infty R(\tau)\cos\omega\tau\,\mathrm{d}\tau$ and $\Psi(\omega)=2\int_0^\infty R(\tau)\sin\omega\tau\,\mathrm{d}\tau$. When $j=k$,

$$\begin{aligned}([\sigma][\sigma]^{\mathrm{T}})_{jj}=&\tfrac{1}{8}\sum_{r=1}^{J}\{(q_{jr}^{11}q_{jr}^{11}+q_{jr}^{22}q_{jr}^{22}+q_{jr}^{12}q_{jr}^{12}+q_{jr}^{21}q_{jr}^{21})[S(\omega_r-\omega_j)+S(\omega_r+\omega_j)]\\&+2(q_{jr}^{11}q_{jr}^{22}-q_{jr}^{12}q_{jr}^{21})[S(\omega_r-\omega_j)-S(\omega_r+\omega_j)]\}a_r^2\\&+\tfrac{1}{8}\{2(q_{jj}^{11}q_{jj}^{22}+q_{jj}^{12}q_{jj}^{21})[S(0)+S(2\omega_j)]\\&+(q_{jj}^{11}q_{jj}^{11}+q_{jj}^{22}q_{jj}^{22}-q_{jj}^{12}q_{jj}^{12}-q_{jj}^{21}q_{jj}^{21})[S(0)-S(2\omega_j)]\}a_j^2,\end{aligned}$$

$$\begin{aligned}([\sigma][\sigma]^{\mathrm{T}})_{j(j+J)}=&\tfrac{1}{8}\{2(q_{jj}^{11}q_{jj}^{12}-q_{jj}^{22}q_{jj}^{21})[S(0)+S(2\omega_j)]\\&+(-q_{jj}^{11}q_{jj}^{21}+q_{jj}^{22}q_{jj}^{12}-q_{jj}^{12}q_{jj}^{11}+q_{jj}^{21}q_{jj}^{22})[S(0)-S(2\omega_j)]\}a_j\\=&([\sigma][\sigma]^{\mathrm{T}})_{(j+J)j},\end{aligned}$$

$$\begin{aligned}([\sigma][\sigma]^{\mathrm{T}})_{(j+J)(j+J)}=&\tfrac{1}{8}\sum_{r=1}^{J}\{(q_{jr}^{11}q_{jr}^{11}+q_{jr}^{22}q_{jr}^{22}+q_{jr}^{12}q_{jr}^{12}+q_{jr}^{21}q_{jr}^{21})[S(\omega_r-\omega_j)+S(\omega_r+\omega_j)]\\&+2(q_{jr}^{12}q_{jr}^{21}-q_{jr}^{11}q_{jr}^{22})[S(\omega_r-\omega_j)-S(\omega_r+\omega_j)]\}\left(\frac{a_r}{a_j}\right)^2\\&+\tfrac{1}{8}\{2(q_{jj}^{11}q_{jj}^{22}+q_{jj}^{12}q_{jj}^{21})[S(0)+S(2\omega_j)]\\&+(-q_{jj}^{11}q_{jj}^{11}-q_{jj}^{22}q_{jj}^{22}+q_{jj}^{12}q_{jj}^{12}+q_{jj}^{21}q_{jj}^{21})[S(0)-S(2\omega_j)]\}.\end{aligned}$$

## References


[1] W. Carnegie, J. Thomas, The coupled bending–bending vibrations of pretwisted, tapered blading, Journal of Engineering for Industry 94 (1972) 255–266.

[2] J.S. Rao, Flexural vibration of pretwisted tapered cantilever beams, Journal of Engineering for Industry 94 (1972) 343–346.

[3] K.B. Subrahmanyam, J.S. Rao, Coupled bending–bending vibrations of pretwisted tapered cantilever beams treated by Reissner method, Journal of Sound and Vibration 82 (1982) 577–592.

[4] K.B. Subrahmanyam, S.V. Kulkarni, J.S. Rao, Coupled bending–bending vibrations of pretwisted cantilever blading allowing for shear deflection and rotary inertia by Reissner method, International Journal of Mechanical Science 23 (1981) 517–530.

[5] M. Swaminathan, J.S. Rao, Vibrations of rotating, pretwisted and tapered blades, Mechanism and Machine Theory 12 (1977) 331–337.

[6] E.B. Magrab, D.E. Gilsinn, Buckling loads and natural frequencies of drill bits and fluted cutters, Journal of Engineering for Industry 106 (1984) 196–204.

[7] O. Tekinalp, A.G. Ulsoy, Modeling and finite element analysis of drill bit vibrations, Journal of Vibration, Acoustics, Stress, and Reliability in Design 111 (1989) 148–155.

[8] O. Tekinalp, A.G. Ulsoy, Effects of geometric and process parameters on drill transverse vibrations, Journal of Engineering for Industry 112 (1990) 189–194.

[9] C.-L. Liao, Y.-H. Dang, Structural characteristics of spinning pretwisted orthotropic beams, Computers and Structures 45 (1992) 715–731.

[10] C.-L. Liao, B.-W. Huang, Parametric instability of a spinning pretwisted beam under periodic axial force, International Journal of Mechanical Science 37 (1995) 423–439.

[11] Y.K. Lin, G.Q. Cai, Probabilistic Structural Dynamics: Advanced Theory and Applications, McGraw-Hill, New York, 1995.